ADVANCED MATERIALS
www.advmat.de

Carbon Dot-Linked Hydrogel for TAMs Transform: Spatiotemporal Manipulation to Reshape Tumor Microenvironment

*Lingyun Li, Jun Wu, Xue Wu, Zhenjian Li, Xianming Zhang, Zekun Yan, Yingqi Liang, Caishi Huang, and Songnan Qu**

As one of the most crucial immune cells in the tumor microenvironment (TME), regulating tumor-associated macrophages (TAMs) is vital for enhancing antitumor immunity. Here, an injectable carbon dots (CDs)-linked egg white hydrogel was developed, termed TAMs Transform Factory (TTF-L-C), to spatiotemporally manipulate TAMs. The fabricated CDs significantly promoted macrophage migration. Notably, TTF-L-C achieved macrophage spatial enrichment through CDs-induced directional recruitment with molecular Ctnnd1 upregulation. Subsequently, the recruited macrophages were locoregionally reprogrammed within TTF-L-C, as well as blocking the upregulated PD-L1. Finally, through multi-stage regulation at spatial, cellular, and molecular levels, TTF-L-C released immune-activated M1 macrophages to the tumor site as it degraded. Moreover, TTF-L-C promoted dendritic cell (DCs) maturation and further boosted T cell activation, thereby reshaping the tumor-suppressive TME. Through peritumoral injection, TTF-L-C enhanced tumor immunotherapy in both subcutaneous and recurrent 4T1 tumor models with satisfactory biosafety. Therefore, TTF-L-C is proposed to become a safe and powerful platform for various biomedical applications.

1. Introduction

Accumulating evidence has suggested that immune suppression in the tumor microenvironment (TME) represents a major barrier to maximizing the clinical potential of immunotherapies.[1] Tumor-associated macrophages (TAMs) are one of the most important immune populations in TME, primarily manifested as a protumoral M2-like phenotype, which can promote tumor angiogenesis, progression, and metastasis.[2] Accordingly, increasing the tumoricidal M1-like macrophages is the key to regulating TAMs and further reshaping TME.[3] TAMs reprogram strategies, especially delivering immunogenic stimulants like lipopolysaccharide (LPS) to polarize macrophages into the M1 phenotype have been developed for decades.[4] During the reprogramming process, ensuring sufficient concentration of immunogenic stimulants localized to the tumor site is of critical significance.[5] Because the overtreated drugs would affect macrophages throughout the whole body, which may cause severe side effects like immune dysregulation and even life-threatening.[6] Indeed, there have already been reported many elegant delivery systems to alleviate immunogenic stimulant overuse through controlling drug release.[7] These paradigms are correct while still limited with off-target effects and systemic drug leakage, which may lead to inefficient immune-activated macrophage accumulation against tumors and even tumor recurrence. Thus, beyond controllable drug release, focusing on macrophage localization, spatially enriching macrophages to achieve locoregionally transformation can improve the biosafety and efficiency of TAMs reprogramming and further immunosuppression reverse. So it is necessary to develop a mildly sequential

L. Li, J. Wu, X. Wu, Z. Li, X. Zhang, Z. Yan, Y. Liang, S. Qu
Joint Key Laboratory of the Ministry of Education
Institute of Applied Physics and Materials Engineering
University of Macau
Taipa, Macau SAR 999078, P. R. China
E-mail: songnanqu@um.edu.mo

The ORCID identification number(s) for the author(s) of this article can be found under https://doi.org/10.1002/adma.202420068

DOI: 10.1002/adma.202420068

S. Qu
Department of Physics and Chemistry
Faculty of Science and Technology University of Macau
Macao SAR 999078, P. R. China

S. Qu
MOE Frontier Science Centre for Precision Oncology University of Macau
Macao SAR 999078, P. R. China

S. Qu
Zhuhai UM Science and Technology Research Institute
Zhuhai 519031, P. R. China

C. Huang
Faculty of Health Science
University of Macau
Taipa, Macau SAR 999078, P. R. China

platform to realize macrophage recruitment followed by locoregional reprogramming to supplement antitumor macrophages. Besides, TAMs reprogramming might increase the expression of the immune checkpoint proteins like programmed death-ligand 1 (PD-L1), which could inhibit the antigen presentation efficacy of macrophages, as well as suppress the activity of T cells.[8] Thus, to comprehensively transform TAMs, a spatiotemporal controllable platform with satisfactory biocompatibility is required to achieve: i) mildly recruit macrophages without intense immune response, ii) locoregionally reprogram macrophages to reduce the systemic leakage of LPS as well as PD-L1 blockade and iii) safely degrade to release the transformed M1 macrophages into tumors for reversing tumor-induced immunosuppression.

Carbon dots (CDs) are emerging carbon-based nanoparticles with ultrasmall size (<10 nm), good fluorescence properties, nontoxicity, low cost, and abundant surface groups for further functionalization, which have been used for antitumor therapy.[9] Actually, CDs synthesized from various raw materials with different surface groups may interact with proteins to regulate their expression and obtain more biological functions, such as macrophage recruitment.[10] Through rational engineering, CDs-constructed nanoplatforms like hydrogels can further promote the development of tumor immunotherapy strategies. Hydrogels especially derived from natural materials, have been widely used to regulate antitumor immunity.[11] These biocompatible hydrogels are usually biologically inert and mainly serve as drug delivery carriers to directly release drugs at the tumor site through peritumoral injection or implantation, thus tandem multiple biological processes.[12] Notably, egg white-based hydrogels have been demonstrated as effective and biologically active extracellular matrix (ECM) mimics to culture and guide cell behaviors, such as 3D scaffolds for cell proliferation.[13] Considering the contained various biologically active compounds in the natural chicken egg white, such as polysaccharides which can recruit macrophages, the chicken egg white-derived hydrogels are promising candidates as biosafe platforms to regulate TAMs.[14] However, natural chicken egg whites are prone to sensitization and require thermal treatment for in vivo application. In addition, the natural chicken egg white-derived hydrogels are usually prepared with relatively high protein concentration through the thermal induced-gelation process, which can cause high cross-linking of protein chains, resulting in an inability to inject and ineffective release of the contained natural bioactive components.[15] Indeed, several CDs-involved natural polymer hydrogel systems have been reported.[16] These hydrogels are usually formed by cross-linking CDs with natural products, such as cellulose and chitosan with good biocompatibility and low cytotoxicity.[17] Thus, it is feasible to employ CDs as the potential nanolinker to fabricate chicken egg white-derived hydrogels in dilute aqueous solution as an effective nanoplatform for TAMs-related tumor immunoregulation.

Herein, we constructed an injectable CDs-linked egg white hydrogel via a thermally induced gelation process, in which the CDs can significantly promote macrophage migration. This CDs-linked egg white hydrogel could be used to locoregionally manipulate TAMs, and we vividly named it a TAMs transform factory (TTF). When encapsulated with LPS and PD-L1 blockade CA170, this composite hydrogel (TTF-L-C) can realize cascade spatiotemporal TAMs transformation to reshape TME for boosting tumor immunotherapy (**Scheme 1a**). Specifically, at the spatial level, TTF released CDs to induce macrophage directional migration by upregulating the macrophage migration-associated gene Ctnnd1 along with activating the Wnt/Ctnnd1/Myc pathway to enrich macrophages (Scheme 1b). Subsequently, the recruited macrophages were locoregionally engineered by LPS and CA170. At the cellular level, LPS reprogrammed macrophages into M1 phenotype, meanwhile at the molecular level, CA170 blocked PD-L1 expressed on the macrophage surface (Scheme 1c). As TTF-L-C degraded, the transformed M1-like macrophages were infiltrated into the tumor and boosted T cell activation (Scheme 1d). In addition to increasing the number of tumoricidal macrophages, TTF-L-C also improved dendritic cells (DCs) mature (Scheme 1e). With the activation of multiple immune cells, TTF-L-C achieved TME reshape. Further in the 4T1 tumor-bearing mice model, the peritumoral injection of TTF-L-C stimulated enhanced antitumor immunity in vivo which inhibited tumor growth and recurrence (Scheme 1f).

2. Results

2.1. Preparation and Characterization of CDs

According to our previous work, the CDs were prepared from citric acid and urea in dimethyl sulfoxide by a solvothermal method[18] (**Figure 1a**). As shown in the transmission electron microscope (TEM) image, the diameters of the CDs were ≈5 nm with clear 0.21 nm lattice fringes, which correspond to the (100) plane of graphite (Figure 1b). Next, the optical properties of CDs were also investigated. As shown in the UV–vis absorption spectrum in Figure 1c, the main absorption bands of CDs were ≈550 and 650 nm. Under green light excitation, the CDs exhibited red fluorescence, which can be used to track their cellular uptake and localization. To verify the biological regulation toward macrophages, the cellular uptake of the CDs by different cells was first detected. Mouse mononuclear phage leukemia cell line RAW 264.7 was chosen as the macrophage model, and mouse breast cancer cell line 4T1 was chosen as the tumor cell model. As the confocal laser scanning microscope (CLSM) images shown in Figure 1d, Figure S1 (Supporting Information), the CDs were barely taken up by 4T1 cells, which mainly accumulated on the cell membrane. The CDs were significantly uptaken by RAW 264.7 cells and mouse bone marrow-derived macrophages (BMDMs), as evidenced by the obvious red fluorescence in the cytoplasm. The different distribution of CDs may be due to the stronger phagocytosis of macrophages.[19] The adsorption results after CDs treatment also indicated that macrophages showed much higher cellular uptake of the CDs (Figure S2, Supporting Information). Then the scratch model was employed to verify the cell migration regulation ability induced by the CDs. The result showed that CDs significantly promoted macrophage migration, however, the migration of 4T1 cells was moderate (Figure 1e, Figure S3, Supporting Information). Furthermore, the transwell model also verified that after 24 h treatment, RAW 264.7 cells migrated significantly compared to the control group (Figure S4, Supporting Information). Besides, the CDs can also promote the proliferation of RAW 264.7 cells with 40% cell number increase at a low concentration of 50 ppm, while causing a 20% cell number decrease in 4T1 cells (Figure 1f). Since it is

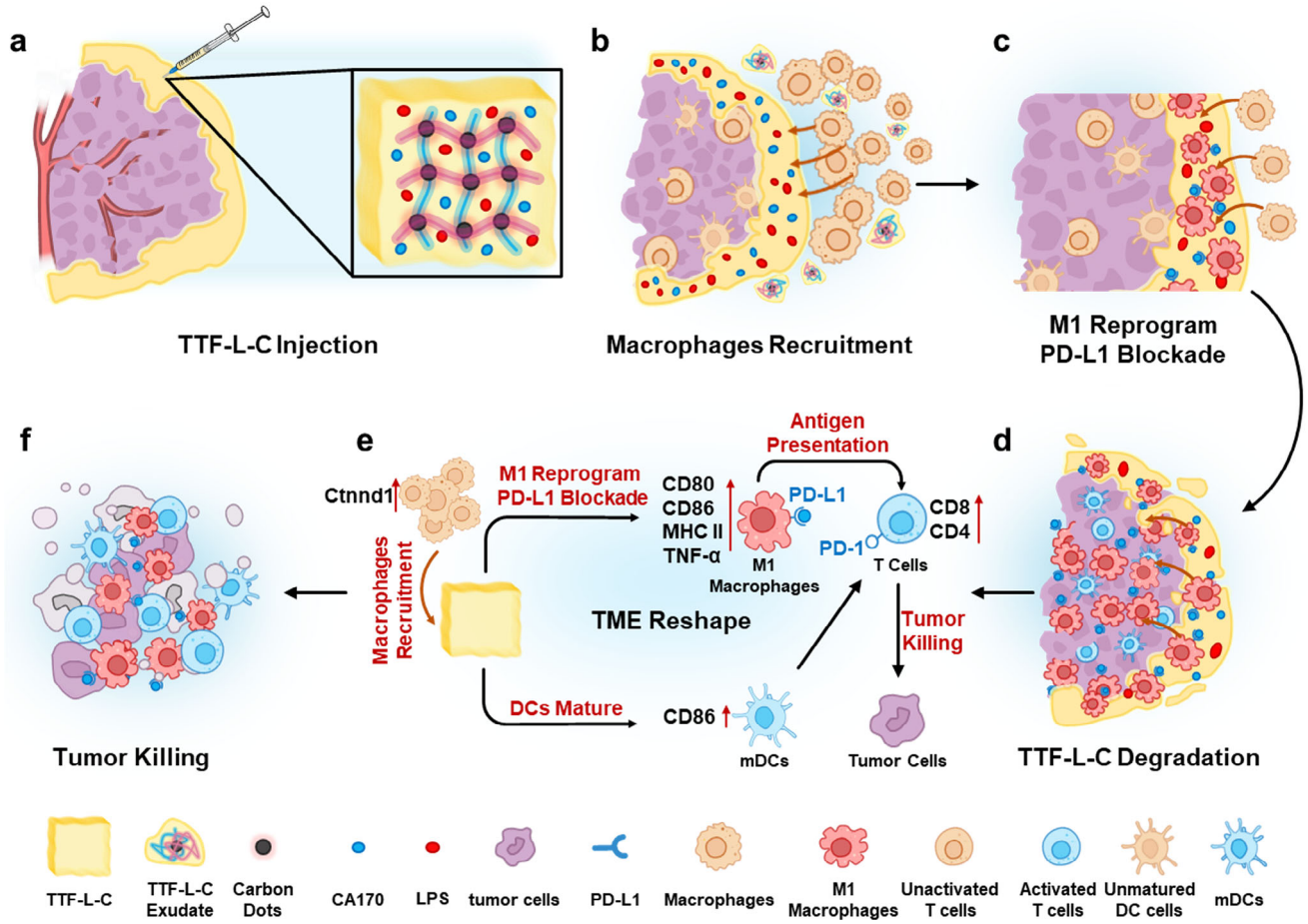

Scheme 1. Schematic illustration of the TTF-L-C spatiotemporally transformed TAMs to reshape TME for tumor immunotherapy. a) Possible structure of the injectable TTF-L-C. b) TTF-L-C specifically recruited macrophages at the spatial level. c) TTF-L-C locoregionally reprogrammed macrophages at the cellular level as well as blocking PD-L1 at the molecular level. d) TTF-L-C degraded to release the transformed macrophages into the tumor site. e) TTF-L-C matured DCs and activated T cells to reshape TME. (f) TTF-L-C inhibited tumor growth and recurrence.

difficult to fix the CDs solution on one side, we designed a culture dish tilting assay to study CDs-induced macrophage directional migration. As shown in Figure S5 (Supporting Information), the bottom of the culture dish was tilted to simulate the CDs solution fixing one side. After 24 h treatment, the cell viability was first measured by CCK-8, and the results showed that CDs promoted macrophage proliferation. Then, the distribution of macrophages was observed under the microscope. The liquid boundary caused by tilting was clearly visible. However, even though the overall cell numbers after CDs incubation were increased, the boundary cell numbers significantly decreased, with the cell numbers on the CDs liquid side increasing, which can be evidence of boundary cells directly migrating to the CDs solution side. All these results demonstrated that the CDs can specifically induce macrophage migration and proliferation in vitro.

2.2. Preparation and Characterization of TTF

Employing the CDs as nano-crosslinkers to prepare thermally induced natural egg white hydrogels can not only improve bioavailability and biosafety but also sequentially control the complex TAMs regulation. In our previous work, we successfully prepared a CDs-linked egg white hydrogel which was used for wound healing.[20] As shown in **Figure 2**a, the preparation process of CDs-linked chicken egg white hydrogel (TTF) was facile to fabricate. TTF was fabricated by mixing CDs in chicken egg white diluted aqueous solution followed by heating in boiling water for 10 min. In contrast, under the same reaction conditions, the pure dilute chicken egg white aqueous solution remained in a liquid state and failed to form a hydrogel, highlighting the crucial crosslinking role of CDs in TTF formation (Figure S6, Supporting Information). The obtained hydrogel was light yellow and transparent, which exhibited red fluorescence due to the composed CDs (Figure 2b,c). As shown in Figure S7 (Supporting Information), the absorption bands of TTF were accompanied by an extended tail into the near-infrared region. This phenomenon could be attributed to the formation of supramolecular structures within the hydrogel, leading to enhanced light scattering. In addition, reducing CDs will make the egg white solution remain in a viscous liquid state, which was unable to gel. Therefore, it is speculated that TTF gelation may be the result of the

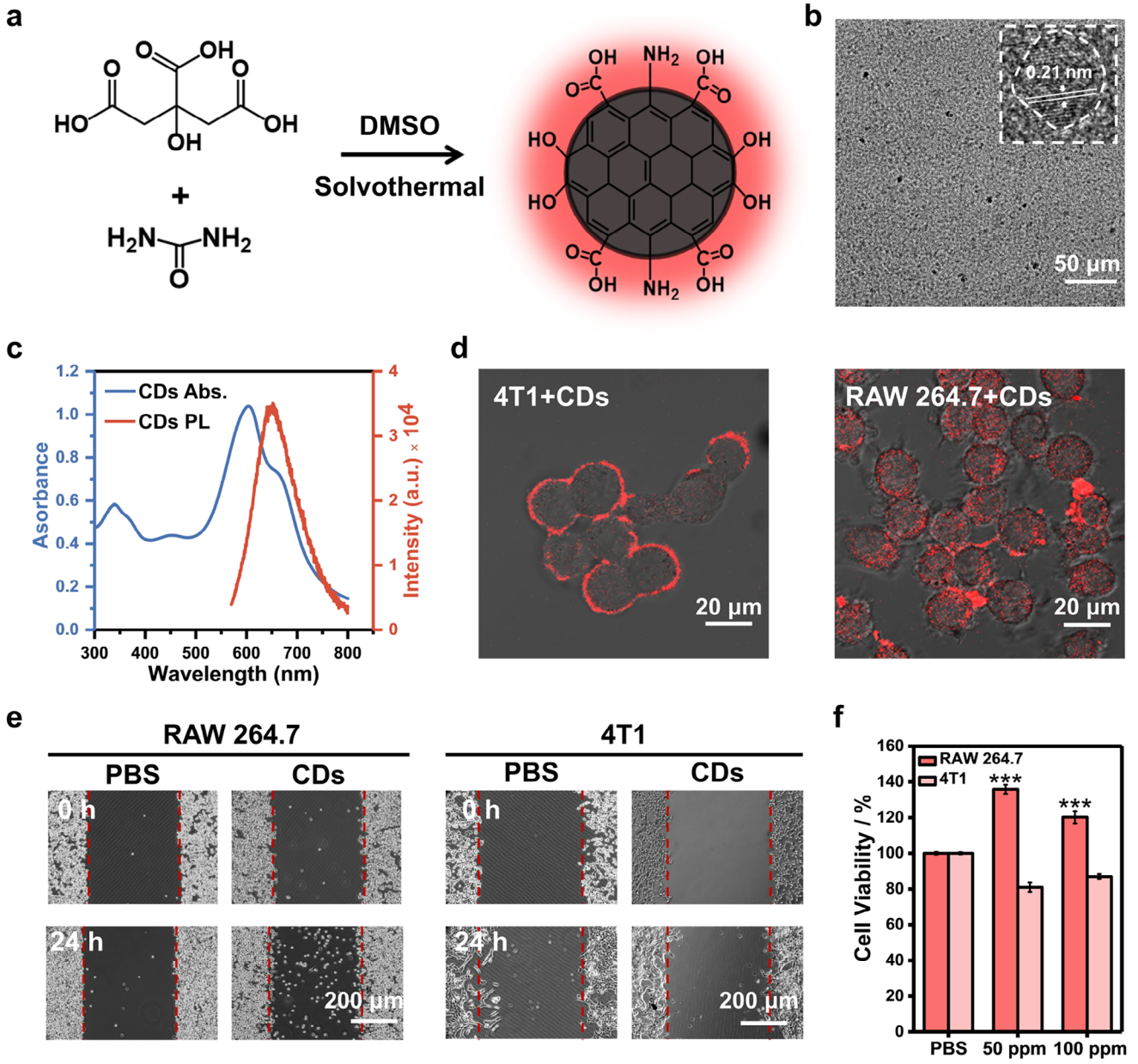

Figure 1. Preparation and characterization of CDs. a) Synthesis process of CDs. b) TEM and HRTEM (inset) images of CDs. c) UV–vis absorption spectrum and PL spectra under 561 nm excitation of CDs. d) CLSM images of 4T1 cells and RAW 264.7 cells treated with CDs. e) RAW 264.7 cells and 4T1 cells migration in the scratch model treated with CDs. f) RAW 264.7 and 4T1 cell viability after CDs treatment at 50 and 100 ppm. Data were all presented as mean values ± SD ($n = 3$). Symbol legend: (*) $p \leq 0.05$, (**) $p \leq 0.01$, (***) $p \leq 0.001$ via the one-way ANOVA.

interaction between CDs and peptides after protein hydrolysis to form a supramolecular network. The rheological properties of TTF prepared with different contents of CDs were tested (Figure S8, Supporting Information). With the addition of CDs, the viscosity was increased, indicating it was more suitable for uniform cell dispersion and culturing. Besides, the storage modulus (G′) was found to be significantly higher than the corresponding loss modulus (G″) when measured through amplitude sweep experiments at a constant frequency of 1 Hz, thereby confirming the elastic properties of the hydrogels, indicating improved stability. The TTF xerogel presented a porous interconnected structure, suggesting that the confined and compact network was formed by the covalent and supramolecular interactions between CDs and the protein chains (Figure 2d). Next, the swelling rate and porosity of TTF were measured, the high swelling rate and porosity indicated good water absorption capabilities and drug loading ability (Figure 2e). Then, to simulate the physiological environment of TTF in vivo, TTF was soaked in PBS to analyze its exudate. From 0 to 24 h, the absorption intensities of the TTF soaking solution were gradually increased, which implicated that TTF gradually decomposed and released the exudate (Figure 2f). The TTF exudate was observed to be porous blocks of about 20–50 μm

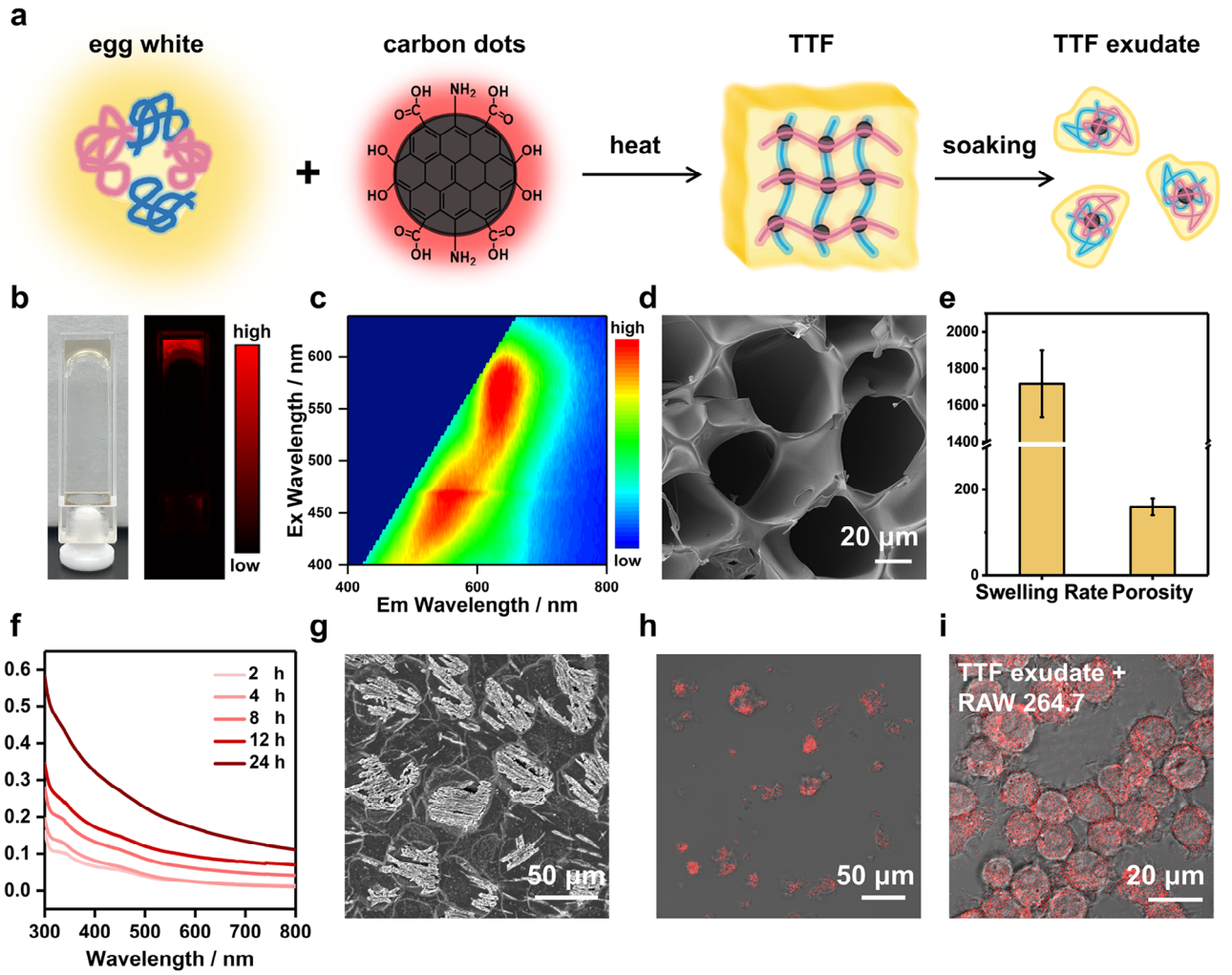

Figure 2. Preparation and characterization of TTF. a) Synthesis process of TTF. b) Bright field and fluorescence images of TTF under 589 nm excitation. c) Excitation-emission map of TTF. d) SEM image of TTF xerogel. e) Swelling rate and porosity results of TTF. Data were presented as mean values ± SD ($n = 3$). f) UV–vis absorption spectra of TTF releasing CDs at different times. g) SEM image of TTF exudate. h) CLSM image of TTF exudate. i) CLSM image of RAW 264.7 cells uptaking CDs released from TTF.

under the scanning electron microscope (SEM) (Figure 2g). Similar to TTF, the TTF exudate also exhibited red PL, indicating the CDs composited egg-white microparticles were gradually released from the TTF (Figure 2h). After incubating the TTF exudate with RAW 264.7 cells, significant red fluorescence can be detected from the macrophages under CLSM, indicating a similar macrophage cellular uptake behavior with the CDs (Figure 2i).

2.3. Macrophages Recruitment by TTF

In order to increase the proportion of tumoricidal M1-like macrophages at tumor sites, regulating the spatial distribution of macrophages with locoregionally transformation is a promising approach. Indeed, it has already been reported that some nanomaterials can spatially regulate TAMs, such as $Gd@C_{82}(OH)_{22}$ and oxidized multiwalled carbon nanotubes (o-MWCNTs).[21] However, these nanomaterials can only prevent the TAMs accumulation but cannot induce macrophage directional migration. Thus, developing nanoplatforms to specifically recruit macrophages toward TME with satisfactory biosecurity and even for further engineering can be a new strategy for TAMs regulation.

To validate the macrophage recruiting capacity of TTF, a transwell migration assay was employed. As shown in **Figure 3**a, RAW 264.7 cells were nested in the upper layer, and a patch of TTF was placed in the lower layer to induce cell migration. After 48 h, the observation results revealed that TTF significantly induced macrophage directional migration compared to the control group (Figure 3b). Hence, more accurate quantitative analysis also demonstrated that TTF induced nearly three times the number of migration macrophages than the PBS group (Figure 3c). Consistently, CDs and TTFs could also induce BMDMs migration (Figure S9, Supporting Information). Then the proliferative ability of the TTF exudate toward different cells was also analyzed. The human embryonic kidney cell line 293T was chosen

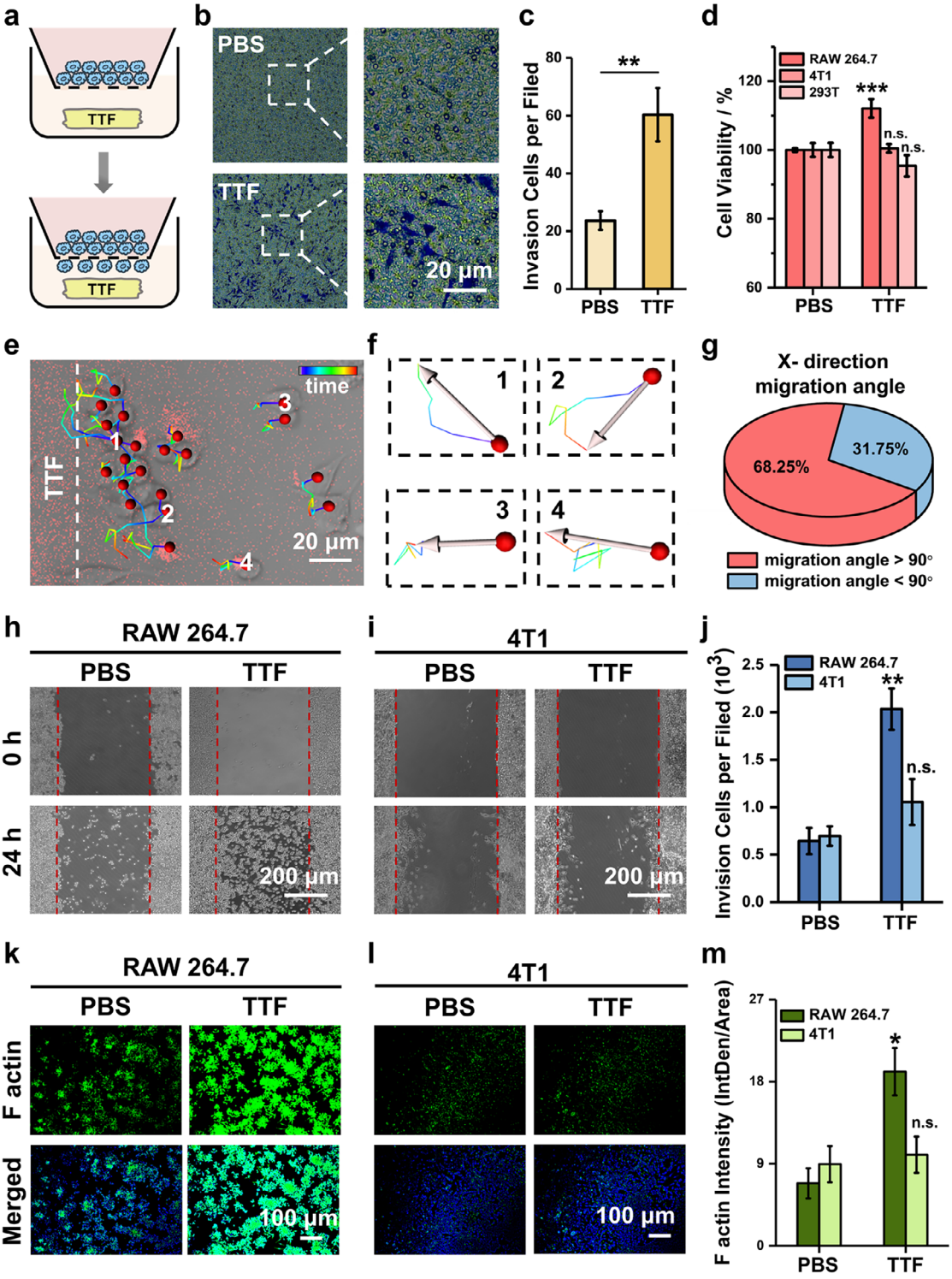

Figure 3. TTF specifically recruited macrophages. a) Schematic illustration of transwell model to verify RAW 264.7 cells migration. b) Crystal violet staining images of RAW 264.7 cells migration after TTF treatment. c) Quantitative analysis results of RAW 264.7 cells migration in transwell assay. d) RAW 264.7, 4T1, and 293T cells viabilities after TTF treatment. e) Migration tracks of RAW 264.7 cells treated with TTF (the red fluorescent signals were from the TTF and TTF extrudate). f) Representative RAW 264.7 cells migration direction. g) Proportions of RAW 264.7 cells in each X-direction migration angle ($n = 65$). h) RAW 264.7 cells and i) 4T1 cells migration in the scratch model after PBS and TTF treatment. j) Quantitative analysis of RAW 264.7 and 4T1 cell migrations in the corresponding scratch assays. CLSM images of k) RAW 264.7 cells and l) 4T1 cells after F actin staining (green color and blue color represented F actin and nucleus, respectively). m) Quantitative analysis of F actin fluorescence intensity of RAW 264.7 and 4T1 cells after TTF treatment. Data were all presented as mean values ± SD ($n = 3$). Symbol legend: (*) $p \leq 0.05$, (**) $p \leq 0.01$, (***) $p \leq 0.001$ via the one-way ANOVA.

as the normal cell model. TTF exudate was collected by immersing TTF (4 × 4 × 0.2 cm) in 5 mL PBS for 72 h. Different cells were incubated with TTF exudate for 48 h, and the CCK-8 results showed TTF had no cell-killing effect on 293T, with cell viability over 90%, implicating satisfactory biological safety (Figure 3d). More interestingly, TTF exudate did not promote 4T1 cell proliferation, but significantly promoted the proliferation of RAW 264.7 cells by ≈10% increment, suggesting that TTF may be beneficial for TAMs to survive in tumor sites (Figure 3d). To more intuitively analyze the tropism of TTF-induced macrophage migration, we placed TTF on one side of the RAW 264.7 cell culture dish and observed the movement of the RAW 264.7 cells every 5 min for 4 h. According to auto-depiction, the movement trajectories of all cells were confirmed (Figure 3e). Most cells moved toward TTF, and some have even migrated into TTF (Figure 3e,f). Moreover, statistical results showed that within 4 h, 68.25% of RAW 264.7 cells had been recruited and tended to migrate toward TTF (Figure 3g).

To further confirm that macrophages could be recruited and proliferated by TTF, the scratch assay was performed. The result showed that TTF significantly promoted macrophage migration with a 4-fold increase (Figure 3h,j). However, the number of migrating 4T1 and 293T cells was moderate, demonstrating that TTF could specifically induce macrophage migration (Figure 3i,j, Figure S10, Supporting Information). Moreover, at the molecular level, CLSM images of the cytoskeletal F actin protein could be another evidence. Compared with 4T1 and 293T cells, the fluorescence intensity of F actin in RAW 264.7 cells increased nearly two times after TTF treatment, illustrating the increased F actin expression as well as the enhanced motility thereby promoting their migration ability (Figure 3k,m; Figure S11, Supporting Information). In addition, macrophages internalizing CDs into the cytoplasm may also cause cytoskeletal rearrangements. TTF treatment can remodel the ECM, further affecting actin expression. In contrast, the fluorescence intensity of F-actin in 4T1 and 293T cells scarcely increased (Figure 3l; Figure S12, Supporting Information). All the above results demonstrated that TTF can specifically recruit RAW 264.7 cells by increasing their migration and proliferation.

Further, the macrophage migration and proliferation induced by egg white hydrogels without CDs were tested (Figure S13, Supporting Information). The CCK-8 results showed that egg white can slightly promote cell proliferation, which may be attributed to the presence of polysaccharides, proteins, and other components in egg white, providing nutritional support for cell growth. Similarly, in the scratch model, egg white could also slightly promote macrophage migration, but the migrated cell number was significantly lower than CDs-incubated cells. In conclusion, these results suggest that egg white, as part of the TTF composition, can promote macrophage proliferation and migration due to the nutrients it contains, but the efficiency was evidently lower than CDs. CDs are the main contributors to TTF recruiting macrophages.

2.4. The Mechanism of TTF Recruiting Macrophages

Generally, ECM is one of the most critical factors for TAMs proliferation, migration, and differentiation. Within the TME, the properties, stiffness, and matrix molecules of ECM can greatly influence cell biological behavior.[22] For instance, Matrix Metalloproteinase-9 (MMP-9) is one of the important factors in ECM, which can affect the migration rate of macrophages.[23] Therefore, the expression of MMP-9 gene in macrophages cultured with TTF was analyzed. As shown in Figure S14 (Supporting Information), there was limited expression of MMP-9 gene in untreated RAW 264.7 cells, but its expression in TTF-cultured RAW264.7 cells was increased by 4-fold, which could reduce cell adhesion and ECM viscosity to enhance macrophage migration.

The RNA-sequencing (RNA-seq)–based transcriptomic analysis was employed to specifically investigate TTF-cultured macrophages. First, statistics data were collected on all altered genes, and one of the most significantly altered genes, Ctnnd1, attracted attention (**Figure 4**a). As an intermediate gene in the Wnt/Myc pathway, Ctnnd1 can express catenin protein to affect cell maturation and movement[24] (Figure 4b). It is worth noting that the Wnt/Myc pathway has already been confirmed to be involved in macrophage migration and recruitment.[24,25] Hence, the gene set enrichment analysis (GSEA) enrichment analysis was performed to analyze the enrichment of the Wnt/Ctnnd/Myc pathway genome. As displayed in Figure 4c, this pathway was significantly enriched in the whole genome, with a normalized enrichment score reaching 1.81 and p-value < 0.001, which was suggested to be related to TTF recruiting macrophages. Consistently, the expression of genomes in the Wnt/Ctnnd1/Myc pathway was plotted as a heat map, and the results demonstrated that TTF can significantly upregulate their expressions (Figure 4d). Then the specific markers related to macrophage phenotyping were examined to evaluate whether macrophage recruitment could affect polarization. The results showed that the M2 phenotype marker CD206 was rarely expressed whether before or after TTF treatment, while the expression of the M1 phenotype marker CD80 was even slightly increased (Figure 4d; Figure S15, Supporting Information). Indeed, according to the previous reports, the Wnt/Myc pathway activation might induce the tendency of M2 polarization. However, we observed that in this TTF-mediated macrophage recruiting system, the expression of inflammation-related nuclear factor kappa-light-chain-enhancer of activated B cells (NFκB) pathway was also enriched, which may neutralize the tendency of M2 polarization (Figure 4d,e).

Furthermore, the CDs regulation of Ctnnd1/Wnt/Myc pathway was examined. First, the Ctnnd1 expression in macrophages treated with CDs was analyzed. After 48 h treatment, the flow cytometry results showed CDs significantly upregulated Ctnnd1 with no effect of CDs self-fluorescence, which can be the reason for TTF recruiting macrophages (Figure 4f,g; Figure S16, Supporting Information). In contrast, Ctnnd1 was barely upregulated in 4T1 cells and other immune cells (Figure S16, Supporting Information). And as expected, the expression of Wnt and Myc was also upregulated (Figure S17, Supporting Information). These results demonstrated that CDs induced macrophage migration and proliferation by regulating the Ctnnd1/Wnt/Myc pathway. Next, Ctnnd1 gene was silenced for further verification. Transwell assay and cell viability of siCtnnd1 macrophages were examined. As shown in Figure S18 (Supporting Information), when the Ctnnd1 gene was silenced, the macrophages had reduced mobility and lost their response to CDs stimulation, exhibiting moderate migration. Consistently, the CCK-8 results demonstrated that CDs could not promote the proliferation of Ctnnd1-silenced cells

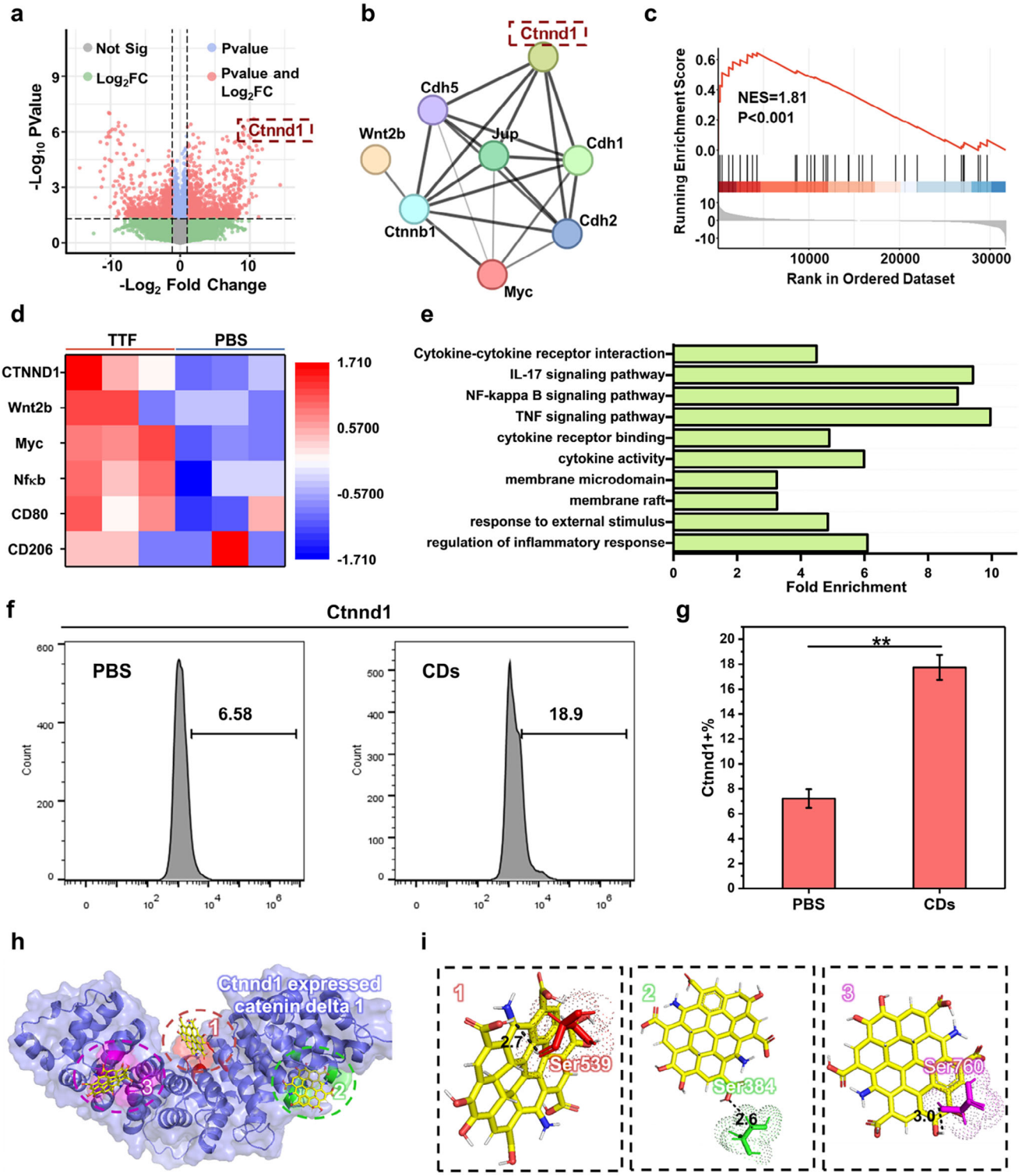

Figure 4. The mechanism of TTF recruiting macrophages. a) Volcano plots of the comparison of TTF-treated and PBS-treated RAW 264.7 cell groups in the RNA-seq results. b) Wnt/Ctnnd1/Myc pathway network. c) GSEA enrichment analysis of Wnt/Ctnnd1/Myc pathway. d) Wnt/Ctnnd1/Myc pathway and macrophage phenotype-related gene alteration heatmap. e) KEGG enrichment analysis. f) Flow cytometry data and g) quantitative analysis of Ctnnd1 expressed catenin delta 1 protein in RAW 264.7 treated with CDs. h) Molecular docking for the simulated CDs toward Ctnnd1 expressed catenin delta 1 protein. i) Hydrogen bonding interactions between the simulated CDs and Ser residues in catenin delta 1 protein.

compared with the normal cells (Figure S19, Supporting Information). All these results indicated that Ctnnd1 is the key to CDs regulating macrophage migration and proliferation. Then, dynamic molecular docking was employed to predict how CDs induce Ctnnd1 upregulation. The predicted CDs structure was composed of 10 benzene rings, with various groups on the surface including amino, carboxyl, and hydroxyl. As shown in Figure 4h,i, the simulated CDs had interactions with the hotspots of Ctnnd1-expressed protein catenin delta 1. More detailed docking results showed that the simulated CDs interacted with the 3 Ser residues of catenin delta 1 through non-covalent bonds mediated by carboxyl and hydroxyl groups, which may prevent protein phosphorylation to reduce its degradation, and this could be one of the reasons for Ctnnd1 upregulation. In summary, the mechanism of the CDs crosslinked TTF-induced macrophage recruitment was explained from two aspects. On the one hand, TTF provided an appropriate ECM environment for TAMs directional movement. On the other hand, CDs can upregulate Ctnnd1, thereby activating the Wnt/Myc pathway and inducing macrophage migration.

2.5. Macrophages Reprogramming by TTF-L-C

Inspired by the successful recruitment by TTF, the recruited macrophages were then reprogrammed locoregionally. To locoregionally increase the concentration of polarizing immunogenic stimulants within the tumor site for better biosafety, several platforms have been reported for delivery, such as "backpacks" and "eMac".[7] These paradigms were mainly focused on controllable local drug release. Here focus on macrophages themselves, with the specific recruitment, TTF-L-C can realize the macrophage spatial enrichment, which would improve the reprogramming efficiency and further enhance the biosafety.

TTF was loaded with different drugs to prepare four different hydrogels (**Figure 5**a). To verify the successful engineering, macrophages were cultured directly on the surface of TTF-L-C to simulate their specific recruitment. Simultaneously, the cell morphology after culturing for 48 h was observed. Compared with the control group, macrophages cultured on TTF-L or TTF-L-C which loaded with LPS displayed similar morphology to M1 macrophages (Figure 5b). The observation result also verified that macrophages could proliferate unaffectedly on the TTF-L-C surface, emphasizing its biosafety. Moreover, the specific markers of M1 macrophages ($CD80^+$ and $CD86^+$) were detected. As shown in Figure 5c, CD80 fluorescence intensity of macrophages cultured with TTF-L and TTF-L-C was increased. Further flow cytometry data more accurately confirmed the upregulation of CD80 and CD86, indicating the successful polarization toward the M1 phenotype (Figure 5d; Figure S20, Supporting Information). Similarly, TTF-L-C can also upregulate the population of $CD80^+$ cells in BMDMs (Figure S21, Supporting Information). Besides the TTF surface culturing, the polarization ability of the TTF exudate was also examined. The results proved that TTF-L-C exudate can also polarize macrophages (Figure S22, Supporting Information). Compared with the positive control L+C group, the polarization efficiency was ≈50%, while the efficiency of macrophages directly cultured on TTF reached 80%. This improved efficiency explicated the necessity of macrophage recruitment, which avoided the polarization capacity loss caused by drug release and verified the superiority of locoregionally reprogramming through macrophage recruitment. In addition, the retained polarization capacity of the TTF-L-C exudate suggested that the released LPS could polarize the unrecruited macrophages. All the above results exhibited that macrophages were successfully reprogrammed.

2.6. Macrophages PD-L1 Blocked by TTF-L-C

Macrophages M1 polarization can upregulate PD-L1, and the excessive PD-L1 expression would reduce antigen presentation efficiency.[8a,26] Thus, after macrophages were cultured on TTF-L-C for 48 h, the PD-L1 expression was first tested. As shown in Figure S23 (Supporting Information), compared with the control group, TTF-L upregulated PD-L1, however, TTF-L-C downregulated the excess PD-L1, demonstrating the necessity of loading the PD-L1 blockade CA170. Then, antigen presentation marker major histocompatibility complex class II (MHC II) was measured. The result showed that MHC II expression increased in macrophages after being polarized into the M1 phenotype, which was more conducive to antigen presentation as well as immune activation. Interestingly, compared with TTF-L, TTF-L-C simultaneously released CA170 further improved MHC II abundance, basically consistent with the positive L+C group, which could be attributed to the PD-L1 blockade[8a] (Figure 5e). Hence, the immune factor secreted by macrophages was also analyzed. Tumor necrosis factor-alpha (TNF-α) is a pleiotropic cytokine produced predominantly by M1-like macrophages and could cause apoptosis. As presented in Figure 5f, the secretion of TNF-α was higher than PBS group after macrophages were reprogrammed to M1 phenotype, and further increased after PD-L1 blockade, implicating enhanced antitumor suppression. Macrophages and T cells co-culture system was then employed to test the antitumor effect of TTF-L-C in vitro. As shown in Figure S24 (Supporting Information), after TTF-L-C stimulated macrophages and T cells, the supernatant was transferred to treat tumor cells. The cell viability of both 4T1 and melanoma cell line B16 cells decreased, proving that TTF-L-C can activate immune cells and enhance the antitumor effect. So far, macrophage engineering including reprogramming and PD-L1 blockade has been completed by TTF-L-C. And finally, through sequential regulation including macrophage recruitment, M1 polarization, and PD-L1 blockade, the transformed macrophages were verified to be activated in vitro, which were expected to achieve enhanced tumor immunotherapy effects in vivo.

2.7. TTF-L-C Induced DCs Maturation

Besides macrophages, dendritic cells (DCs) also play a crucial role in both innate and adaptive immune systems.[27] Compared to immature DCs (iDC), mature DCs (mDC) can stimulate T lymphocytes to produce specific antitumor immune responses.[28] During this period, the expression of the co-stimulatory molecule CD86 will be upregulated, suggesting that DCs have been developed into mDCs.[27b] LPS is a TLR4 agonist that is commonly used for DCs maturation. Thus, the TTF-L-C-induced DCs

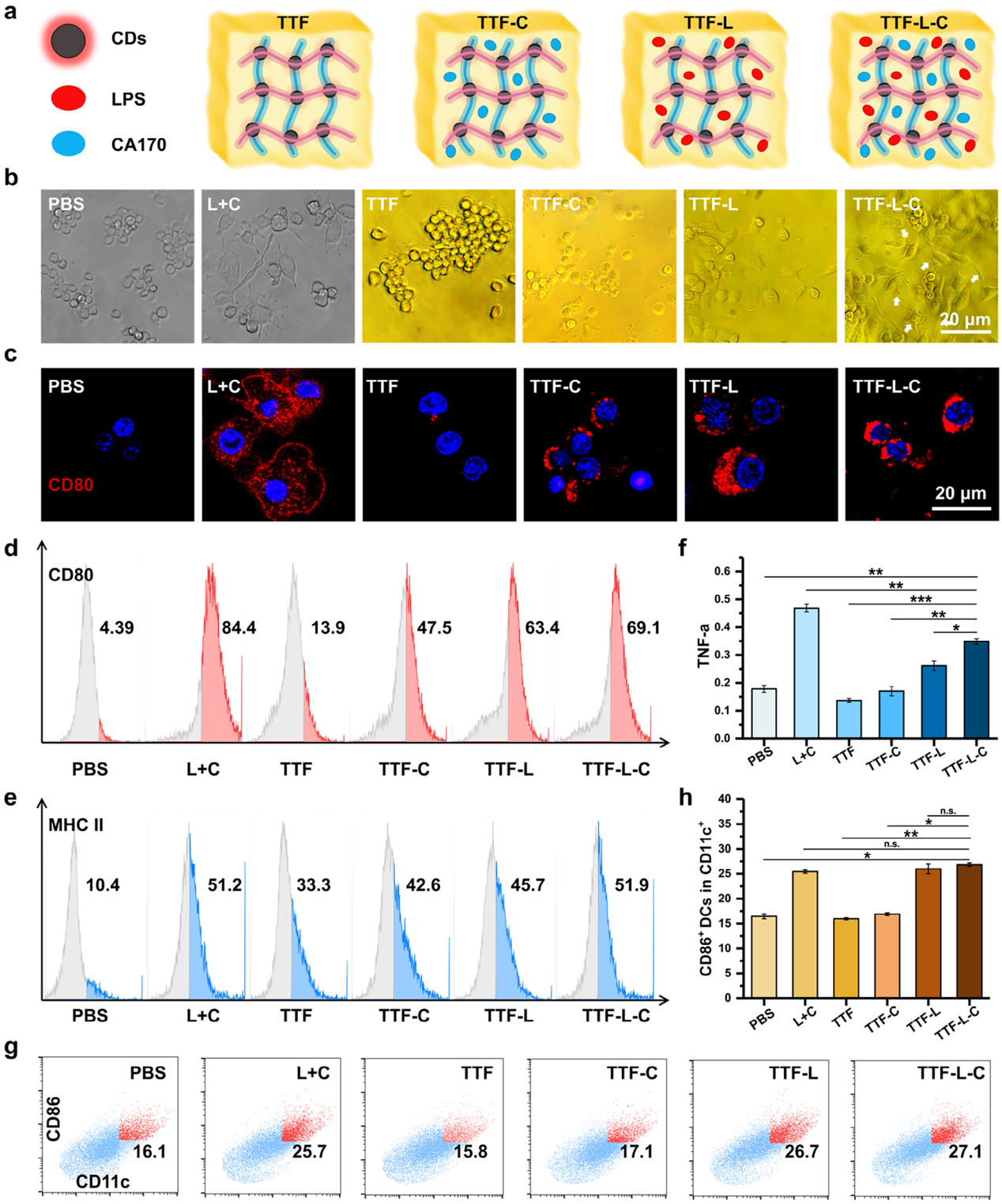

Figure 5. Recruited macrophages engineered by TTF-L-C. a) Schematic illustration of 4 different hydrogels. b) Brightfield images of RAW 264.7 cell morphology after culturing in different conditions (L+C represented LPS / CA170 mixture). c) CLSM images of RAW 264.7 cells with CD80 staining after culturing in different conditions (red color and blue color represented CD80 and nucleus, respectively). Flow cytometry results of d) CD80 and e) MHC II in RAW 264.7 cells after culturing in different conditions. f) TNF-α secreted level in RAW 264.7 cells after culturing in different conditions. g) Flow cytometry results of CD86/CD11c in BMDCs and h) quantitative analysis of $CD86^+$ DCs in $CD11c^+$ DCs treated with different conditions. Data were all presented as mean values ± SD ($n = 3$). Symbol legend: (*) $p \leq 0.05$, (**) $p \leq 0.01$, (***) $p \leq 0.001$ via the one-way ANOVA.

maturation was studied in vitro using the bone marrow-derived dendritic cells (BMDCs) isolated from the Balb/c mice. The TTF-L-C exudate was incubated with BMDCs, and the BMDCs maturation was detected by flow cytometry. The mDCs ($CD86^+$ cells) population in $CD11c^+$ BMDCs after TTF-L and TTF-L-C treatment was significantly higher than the control group, even TTF-L-C group is slightly higher than the positive control L+C group (Figure 5g,h). These results demonstrated that TTF-L-C can also enhance BMDCs maturation and reshape the TME comprehensively.

2.8. Tumor Growth Inhibition by TTF-L-C In Vivo

As shown in **Figure 6**a, TTF-L-C was injectable through a syringe extrusion. Based on the red fluorescent signals, TTF-L-C was subcutaneously injected into a mouse to detect its biodegradability. The result showed that TTF-L-C had excellent biocompatibility and could be completely degraded within 14 days without causing a strong inflammatory reaction, indicating that TTF-L-C was sufficiently biosafe for further TAMs transformation and TME reshaping (Figure 6a).

Since TTF-L-C was proven to activate macrophages in vitro, we subsequently evaluated its tumor immune therapeutic effect in vivo. First, Balb/c mice bearing 4T1 tumors were randomly divided into six groups for 25-day treatments (Figure 6b). Hydrogels were peritumorally injected when the tumor grew to 50 mm^3. The tumor volume of each mouse was recorded the other day (Figure S25, Supporting Information). Compared with the PBS group, single loading of CA170 or LPS in TTF-C and TTF-L treated groups showed moderate tumor growth inhibition efficacy, but dual loading in TTF-L-C treated group evidently improved the treatment effect. After 25-day treatment, TTF-L-C treated group showed the highest tumor growth inhibition effect among all groups (Figure 6c; Figures S26 and 27, Supporting Information), with no obvious influence on the body weight (Figure S28, Supporting Information). Further, staining analysis was performed on the mouse tumor tissues after treatment. As displayed in Figure S29 (Supporting Information), H&E and TUNEL results indicated increased tumor cell necrosis and damage after TTF-L-C treatment. Consistently, TTF-L-C treatment upregulated C-Cas3, which can promote tumor cell death, and downregulated Ki67, which can promote cell proliferation. Hence, immunohistochemistry (IHC) results verified the completed engineering of macrophages through TTF-L-C reprogramming and immune checkpoint blockade(ICB) (Figure S30, Supporting Information). Compared with the PBS group, the TTF-L-C treated group showed increased expression intensity of F4/80, which confirmed that TTF-L-C could successfully recruit macrophages in vivo. Besides, the proportion of M1-like macrophages ($CD86^+$) in tumor tissues treated with TTF-L and TTF-L-C was increased, indicating that macrophage reprogramming was successful. In addition, the increased proportion of $CD4^+$ (a marker of auxiliary T cells) and $CD8^+$ (a marker of cytotoxic T cells) T cells benefited from PD-L1 blockade, which further enhanced immune activation. In addition, the in vivo therapeutic effects of L+C intratumoral injection compared with TTF-L-C were also tested. As shown in Figure S31 (Supporting Information), L+C was injected intratumorally and TTF-L-C was injected peritumorally once, then the tumor growth was observed for 14 days. After 14-day treatment, TTF-L-C also showed the best therapeutic effect among all groups, with the tumor volume and weight being almost half of L+C, indicating TTF as the drug carrier to sustained release drugs can enhance tumor inhibition in vivo (Figure S31, Supporting Information). The blood parameters were also tested after treatment. All the biochemical parameters were not significantly different from the normal mice within the normal range, illustrating that TTF and TTF-L-C had good in vivo biocompatibility (Figure S32, Supporting Information). Besides, in vivo, PD-L1 inhibition was analyzed. For in vivo test, we detected PD-L1 inhibition in M1 macrophages of isolated tumor tissues (Figure S33, Supporting Information). First, M1 macrophages in tumor tissues were identified using F4/80 and CD80. Then, PD-L1 on M1 macrophages were analyzed. Consistent with the in vitro results, TTF-L resulted in PD-L1 upregulation, emphasizing the necessity of PD-L1 blockade using CA170. And TTF-L-C downregulated redundant PD-L1. It is worth noting that TTF-L-C inhibited PD-L1 better than L+C, which also emphasized the significance of TTF.

2.9. Tumor Recurrence Inhibition by TTF-L-C In Vivo

Although surgical resection is currently the first choice of clinical treatment for most solid tumors, postoperative tumor recurrence and metastasis are the main causes of mortality.[29] Therefore, filling the surgical site with fillers such as hydrogels that can sustainably inhibit tumor proliferation has become an effective tumor treatment method.[30] Particularly, breast cancer patients have a great demand for postoperative filling biomaterials.[31] Based on the favorable biocompatibility and immune activation ability of TTF-L-C, we hypothesized that it could serve as the postoperative filling biomaterial. BALB/c mice preloaded with 4T1 breast cancer cells and followed by resection were employed as the animal model. After 14 days of the tumor establishment, we removed ≈90% of an orthotopic 4T1 breast cancer and filled it with hydrogels simultaneously. The BALB/c mice were treated with PBS, LPS / CA170 mixture intravenous injection (L+C i.v.), TTF, TTF-L, TTF-C and TTF-L-C. The time course of the therapeutic efficiency study is depicted in Figure 6d. Tumor relapses appeared rapidly in the PBS-treated mice and L+C i.v.-treated mice, as shown in Figure 6e and Figure S34 (Supporting Information). The TTF-treated mice exhibited slight tumor inhibition, which may be due to recruiting macrophages to the tumor site. After loading the single drug (TTF-L or TTF-C), the postoperative tumor inhibition was further enhanced, while TTF-L-C demonstrated a synergistic effect. After 19-day treatment, TTF-L-C had the most significant effect on inhibiting tumor recurrence (Figure 6e; Figure S35, Supporting Information). More precisely, the mass of the ex vivo tumor tissues was measured. The results displayed in Figure S36 (Supporting Information) demonstrated that the tumor mass treated with TTF-L-C was 20% of that in the PBS group and 30% of that in the L+C i.v. The treated group, confirming its excellent tumor recurrence-preventing capacity after surgery. Besides, no obvious influence showed on body weight, indicating superior biosecurity (Figure S37, Supporting Information). Overall, TTF-L-C can effectively inhibit tumor recurrence in vivo. It is worth noting that these therapeutic effects only depend

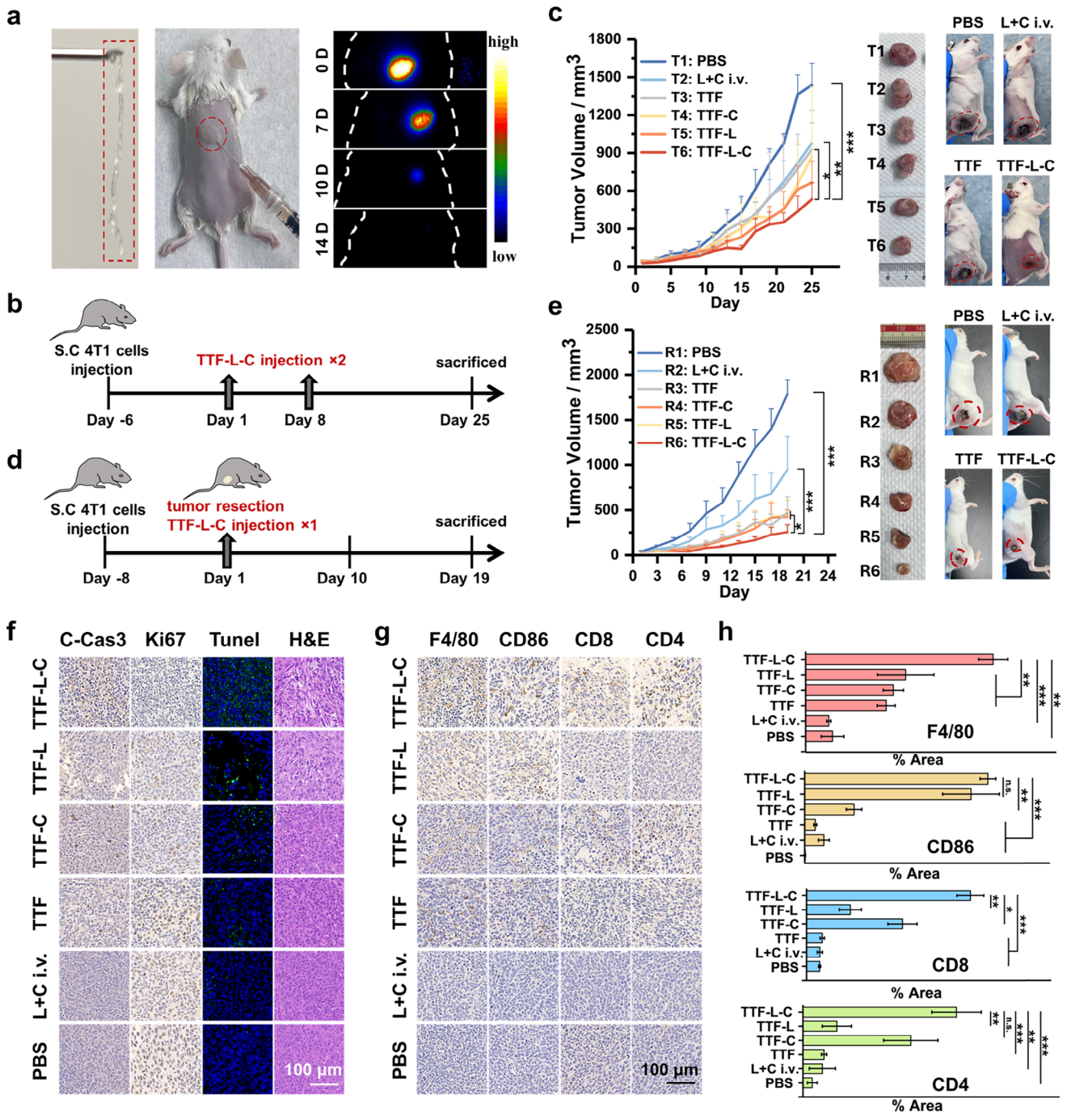

Figure 6. TTF-L-C inhibited tumor growth and recurrence in vivo. a) Images of TTF-L-C subcutaneously injected mice and in vivo fluorescence images at various time points after injection. b) Schematic illustration of TTF-L-C therapy in the tumor growth subcutaneous mouse model. c) Tumor growth curves of T1–T6 groups, representative isolated tumor images, and tumor-bearing mice images on day 25. Data were presented as mean values ± SD ($n = 5$). d) Schematic illustration of TTF-L-C therapy in the tumor recurrence mouse model. e) Tumor growth curves of R1–R6 groups, representative isolated tumor images and tumor-bearing mice images on day 19. Data were presented as mean values ± SD ($n = 5$). f) C-Cas3, Ki67, and H&E staining, as well as TUNEL results of tumor tissue slices from R1-R6 groups. g) IHC staining of F4/80, CD86, CD8 and CD4 of tumor tissue slices from R1-R6 groups. h) Quantitative analysis results of F4/80, CD86, CD8 and CD4 staining of tumor tissue slices from R1-R6 groups. Data were presented as mean values ± SD ($n = 3$). Symbol legend: (*) $p \leq 0.05$, (**) $p \leq 0.01$, and (***) $p \leq 0.001$ via the one-way ANOVA.

on the immunomodulatory effect activated by TTF-L-C with no chemotherapy drugs involved.

Immune responses were activated by TTF-L-C to boost antitumor therapy. And tumor tissue section staining as well as IHC analysis for the recurrence model also noted the superiority of TTF-L-C. First, the expression of C-Cas3 was the highest in the TTF-L-C treated group, indicating increased tumor cell apoptosis. Consistently, the downregulation of Ki67 illustrated that the proliferation ability of tumor cells was significantly reduced compared with the PBS-treated mice. Ultimately, this led to increased cell apoptosis in TUNEL staining and severe damage in H&E staining (Figure 6f), while normal organs (heart, liver, spleen, lung, and kidney) did not show obvious necrosis (Figure S38, Supporting Information). Furthermore, IHC results proved that TTF-L-C killed tumor cells through immune activation (Figure 6g). To verify the ability of TTF to recruit macrophages in vivo, the specific marker F4/80 of macrophages was stained and analyzed. The result showed that compared with mice without TTF implantation, the expression of F4/80 in the TTF-treated mice was expressively increased, implicating that TTF can recruit macrophages in vivo. In addition, after TTF was loaded with LPS, the expression of M1-like macrophage marker $CD86^+$ also increased meaningfully, elucidating that macrophage reprogramming was achieved in vivo. Moreover, PD-L1 blockade CA170 release upregulated CD4 and CD8, and further activated T cell immunity. Quantitative fractionation also gave consistent evidence (Figure 6h). All these results explicated that TTF-L-C can realize its expected TAMs transform function in vivo, and finally achieve enhanced immune activation to suppress tumors.

Next, RNA-seq-based transcriptomics was also employed to verify the tumor recurrence inhibition effects of TTF-L-C at the biological molecular level. In both analyses, L+C i.v., TTF, and TTF-L-C treated tumors were compared with the PBS-treated group as well as TTF-C and TTF-L treated tumors were compared with TTF-L-C group. The heatmap of differential expression genes of these groups was created and the significantly changed gene expressions were counted (**Figure** 7a–c). Then, to give the functional classification for the altered genes, Gene Ontology (GO) analysis and the Kyoto Encyclopedia of Genes and Genomes (KEGG) analyses were performed. According to GO biological processes, the main terms of altered genes in Biological Process (BP), and Molecular Function (MF) have been shown in Figure 7d. Obviously, immune-related pathways, especially genomes related to macrophage antigen presentation, were highly enriched. Coincidentally, KEGG enrichment analysis gave similar results, TTF-L-C can regulate ECM and further activate tumor immunity through TAMs transform (Figure 7e). Hence we observed key genes related to antitumor TAMs protein expression. As shown in Figure 7f, genes that were significantly enriched in GO and KEGG analyses were collected and almost all these genes were related to TAMs-related tumor immunity, which further verified TAMs transform. Compared with L+C i.v.-treated group, TTF-L-C up-regulated the specific marker of macrophages, indicating the increased population of macrophages in the tumor site, (Figure 7g). Besides, compared to single drug loaded TTF-C and TTF-L, the TTF-L-C exhibited enhanced TAMs immune activation capacity, displayed in improved gene expression of M1 macrophage marker gene and T cell activation marker gene, which implicated TTF-L-C synergistic immune regulation effect (Figure 7g). Finally, the activated immune regulation significantly inhibited tumor growth, leading to the downregulation of tumor proliferation-related genes and the upregulation of tumor-killing-related cytokines (Figure 7h). Above all, TTF-L-C showed satisfied TAMs-related tumor immune activation at the RNA level.

3. Conclusion

In summary, we developed a biosafe injectable CDs-linked chicken egg white hydrogel (TTF) encapsulating with LPS and PD-L1 (TTF-L-C) to achieve spatiotemporal TAMs transformation. Remarkably, TTF-L-C can realize macrophage directional recruitment, locoregionally reprogram, and PD-L1 blockade to comprehensively transform TAMs. The synthesized CDs can recruit macrophages by upregulating Ctnnd1. Compared with reported TAMs regulation paradigms, TTF-L-C-induced macrophage spatial regulation not only increased the population of tumoricidal macrophages at the tumor site but also provided a new idea for localized reprogramming to alleviate the side effects of immunogenic stimulants. In terms of therapeutic effect, TTF-L-C achieved TAMs spatial-cellular-molecular multi-stage regulation, sequentially realized TAMs recruitment, localized reprogramming, and ICB to comprehensively transform TAMs for increased immunity. And finally, both 4T1 tumor subcutaneous and recurrence models demonstrated enhanced immunotherapy efficacy. From a methodological perspective, the strategy of loading immunogenic stimulants and immune checkpoint blockades in the TTF provides an effective reference for designing biomimetic antitumor hydrogels. Through rational engineering, the CDs-linked chicken egg white hydrogel can provide a powerful tool for various biomedical applications.

4. Experimental Section

Cell Lines and Animals: Mouse breast cancer cell line 4T1 and mouse mononuclear phage leukemia cell line RAW 264.7 and rat cardiomyocyte cell line 293T were all purchased from the American Type Culture Collection (ATCC). 4T1, RAW 264.7, and 293T cells were cultured in Dulbecco's modified Eagle's medium (Gibco). Ans cells were cultured in media containing 10% FBS (Gibco) and 1% penicillin–streptomycin (BI) at 37 °C in 5% CO2. Female BALB/c mice (6–8 weeks old) were purchased from Zhuhai Bestest Biotechnology Co., Ltd. (Zhuhai, China). Moreover, all mice were maintained in a specific pathogen-free environment. Animal operations complied with ethical standards and were approved by the Animal Care and Welfare Ethics Committee, Institute of Applied Physics and Materials Engineering, University of Macau (ethics number: UMARE-048-2023).

Preparation of CDs: Citric acid (2 g) and urea (6 g) were dissolved in 20 mL of DMSO. The solution was then heated at 160 °C for 6 h under solvothermal conditions. After cooling to room temperature, the solution was purified through dialysis (molecular weight cutoff of 1000 Dalton) for 72 h. Finally, the aqueous solution from the dialysis bag was collected and freeze-dried to obtain CDs.

Preparation of TTF and TTF-L-C: First, 40 mL of chicken egg white was mixed with CDs solution (8 mg mL^{-1}), and the mixture was diluted with pure water (a 1:1.2 volumetric ratio). Then, the mixed solution was centrifuged at 10000 rpm for 10 min to collect the supernatant and remove the insoluble components. LPS (7.4 μg mL^{-1}) and CA170 (60 μg mL^{-1}) were added to the supernatant and heated with a boiling water bath for 10 min to obtain transparent TTF-L-C. For in vitro experiments with TTF-L-C

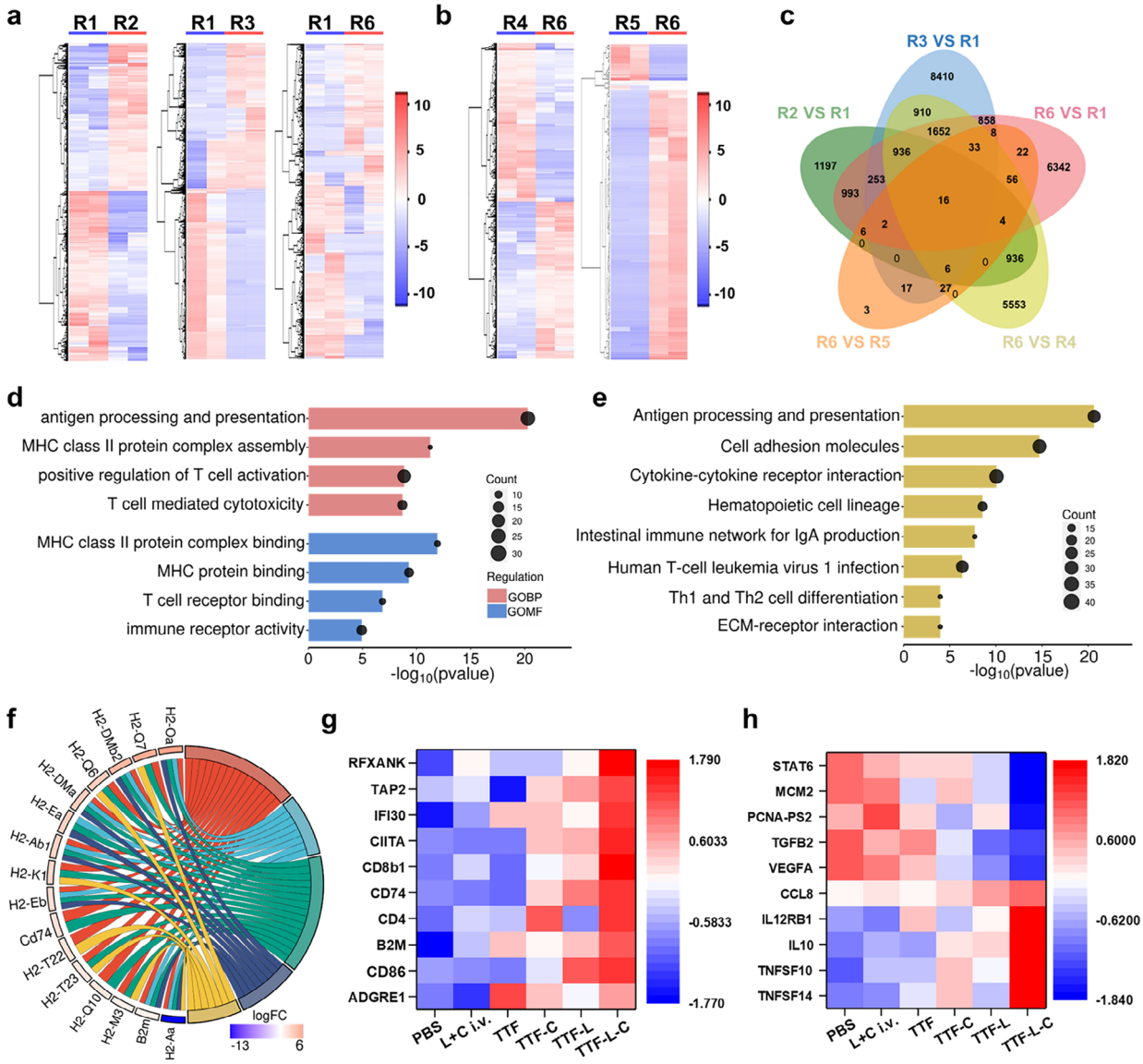

Figure 7. RNA-seq analysis of TTF-L-C treatment in the tumor recurrence mouse model. a) Differential gene heat maps for tumors treated with L+C i.v., TTF or TTF-L-C compared with PBS-treated ones. b) Differential gene heat maps for tumors treated with TTF-C or TTF-L compared with TTF-L-C treated ones. c) Venn plot analysis of significantly altered genes in different groups. d) GOBP and GOMF enrichment analysis of the TTF-L-C treated group compared with the PBS-treated group. e) KEGG enrichment analysis of the TTF-L-C treated group compared with the PBS-treated group. f) Chord plot analysis of the relationship between the significantly altered genes and the enriched pathways. g) Macrophage activation-related gene alternations after treatment with TTF-L-C. h) Tumor proliferation and killing-related gene alterations after treatment with TTF-L-C.

treatment, the LPS dose was 1 μg mL^{-1} and the CA170 dose was 50 nM. For in vivo experiments with TTF-L-C treatment, the LPS dose was 0.3 mg kg^{-1} and the CA170 dose was 0.2 mg kg^{-1}.

Characterization of TTF-L-C Mechanical Properties: i) Swelling rate. First, the prepared hydrogel was freeze-dried for 3 days, and the mass was weighed as Wd, then the freeze-dried hydrogel was soaked in water with a mass of Ws. The swelling rate was calculated as follows:

$$Swelling\ Rate = \frac{Ws - Wd}{Wd} \tag{1}$$

ii) Porosity. First, weigh the freeze-dried hydrogel as m0 and measure the volume as V0. Then the hydrogel was soaked in absolute ethanol until equilibrium, and the mass was recorded as m1. Porosity was calculated as follows:

$$Porosity = \frac{m_1 - m_0}{\rho_{ethanol} \times V_0} \tag{2}$$

Transwell Assay for Macrophage Migration: RAW264.7 cells were inoculated into the upper nest at the density of 105 mL^{-1} and cultured overnight in the incomplete medium. Hydrogel soaking solution was added to the 24-well plate and cultured for 48 h. Then the soaking solution was removed, PBS was added and washed three times, next 4% paraformaldehyde was added to fix for 30 min. After washing again with PBS, crystal violet was added and stained for 30 min. Finally, the cells were washed

with PBS, and the upper layer of nested non-migrated cells was carefully wiped off with a cotton swab for imaging.

Scratch Assay for Macrophage Migration: 4T1, RAW264.7, and 293T cells were seeded in six-well plates at a density of 10^5 mL^{-1} and cultured in a complete medium for 24 h. Discard the culture medium and wash 3 times with PBS, then a 10 µL tip was employed to scratch the bottom of the well plate. The cells were cultured with hydrogel in an incomplete medium immersion solution for 48 h and finally imaged under the microscope.

Cell Imaging Assay: RAW264.7 cells were seeded in confocal dishes at a density of 105 mL^{-1} and cultured overnight. Then, the cells were fixed with 4% paraformaldehyde for 15 min and washed three times with PBS. Next, the cells were incubated with 0.1% triton for 15 min, washed 3 times with PBS, and then incubated with 3% BSA to block the cells for 30 min. After staining cells with phalloidin and Hoechst for 15 min, cells were washed 3 times with PBS and used for confocal imaging.

Flow Cytometry Assay Detected Cell Typing: Cells were cultured on the hydrogel surface or in a hydrogel-soaking solution overnight. Then the cells were digested and dispersed in PBS to obtain a cell suspension, which was washed three times. Next, cells were blocked by incubating with 3% BSA for 30 min. Finally, the cells were incubated with CD80 / CD86 / CD11c antibody for 1 h, washed three times, and then loaded for flow cytometry.

Gene Silence Assay: Seed cells in a 6-well plate at a density that allows them to reach 60%–70% confluence on the day of transfection. Prepare transfection complexes according to the manufacturer's instructions. Typically, this involves diluting siRNA and transfection reagent in serum-free medium, then combining them and incubating for 15–20 min. Add the transfection complexes to the cells and incubate for 4–6 h, then replace with fresh complete medium. Then Incubate the cells for 24–72 h to allow gene silencing. The optimal time depends on the target gene and cell type.

Elisa Assay Detected Cytokine Content: Cells were cultured on the hydrogel surface or in hydrogel-soaking solution overnight. Then the cells were digested and dispersed in PBS to obtain a cell suspension, which was washed three times. Next, IL-2 kit was used to detect the content of IL-2 secreted by cells, and finally microplate reader was employed to measure the absorbance. Macrophages Migration Tracks Analysis and Molecular Docking TTF was fixed on one side of the culture dish, macrophages were cultured for 4 h, and video images were recorded using a confocal microscope. Imaris software was employed to analyze migration tracks. The analysis steps include video import, cell positioning, confirmation of the initial position, intermediate position and final position, and automatic drawing of the cell movement trajectory. The docking process between CDs and Ctnnd1 expressed catenin delta 1 protein was achieved by Discovery Studio software. The crystal structures of catenin delta 1 protein were obtained from PDB. First, the receptor-ligand interactions module was used to dock the CDs into its receptor protein. After initial rough results, the most stable binding pose with the lowest energy was obtained through ligand interaction analysis. Finally, Pymol software was used to plot interaction poses.

Mouse Treatment Scheme: For the tumor recurrence model, mice were randomly divided into six groups ($n = 5$) for 19-day treatments. To construct 4T1 tumor-bearing mice, 1×10^5 4T1 cells (100 µL in PBS) were injected subcutaneously into each mouse. Animals were housed at 22 °C in a 12 h light / dark cycle and fed rodent chow and water freely in SPF space. After 9 days, when the tumor volume reached ≈300 mm^3, remove most of the tumor, leaving rice-sized tumors as recurrent tumors. Meanwhile, the hydrogel was implanted into the subcutaneous tumor site and sutured. During the 19-day treatment, tumor volume and mouse body weight were measured every other day, until the tumor volume grew to ≈2000 mm^3.

Immunohistochemistry of Mouse Tumor Tissue: For CD86, F4/80, CD8, CD4, C-Cas3, Ki67, and TUNEL staining, tissue slides were treated with a kit. In H&E staining, the cryogenic slides with a thickness of 8 µm were continuously treated with 10% v/v formalin (dissolved in PBS) for half an hour. The slides were then washed with DI (deionized) water and alcohol with different concentrations including 100%, 95%, and 70%. The hematoxylin staining was conducted for ≈3 min and was washed with water for ≈1 min. The images were collected with a digital slide scanner.

Supporting Information

Supporting Information is available from the Wiley Online Library or from the author.

Acknowledgements

This work was supported by the Science and Technology Development Fund of Macau SAR (0007/2021/AKP, 0002/2024/TFP, 0139/2022/A3), University of Macau-Dr. Stanley Ho Medical Development Foundation "Set Sail for New Horizons, Create the Future" Grant 2025, the Shenzhen-Hong Kong-Macao Science and Technology Innovation Project (category C) SGDX20210823103803021, and University of Macau-Huafa Group Joint Laboratory (HF-001-2021).

Conflict of Interest

The authors declare no conflict of interest.

Data Availability Statement

The data that support the findings of this study are available from the corresponding author upon reasonable request.

Keywords

carbon dots, hydrogel, macrophage recruitment, macrophage reprogram, tumor immunotherapy

Received: December 19, 2024
Revised: March 20, 2025
Published online: April 3, 2025

[1] a) D. F. Quail, J. A. Joyce, *Nat. Med.* **2013**, *19*, 1423; b) T. Tang, X. Huang, G. Zhang, Z. Hong, X. Bai, T. Liang, *Signal Transduct. Target Ther.* **2021**, *6*, 72.

[2] a) A. Christofides, L. Strauss, A. Yeo, C. Cao, A. Charest, V. A. Boussiotis, *Nat. Immunol.* **2022**, *23*, 1148; b) Y. Cheng, S. Song, P. Wu, B. Lyu, M. Qin, Y. Sun, A. Sun, L. Mu, F. Xu, L. Zhang, J. Wang, Q. Zhang, *Adv. Healthcare Mater.* **2021**, *10*, 2100590; c) J. Condeelis, J. W. Pollard, *Cell* **2006**, *124*, 263; d) B.-Z. Qian, J. W. Pollard, *Cell* **2010**, *141*, 39; e) D. G. DeNardo, B. Ruffell, *Nat. Rev. Immunol.* **2019**, *19*, 369.

[3] a) X. Xu, X. Gong, Y. Wang, J. Li, H. Wang, J. Wang, X. Sha, Y. Li, Z. Zhang, *Adv. Therap.* **2020**, *3*, 1900181; b) J.-H. Sun, X. Liang, M. Cai, L. Yan, Z. Chen, L. Guo, L. Jing, Y. Wang, D. Zhou, *Nano Lett.* **2022**, *22*, 4410; c) X. Zhang, S. Li, I. Malik, M. H. Do, L. Ji, C. Chou, W. Shi, K. J. Capistrano, J. Zhang, T.-W. Hsu, B. G. Nixon, K. Xu, X. Wang, A. Ballabio, L. S. Schmidt, W. M. Linehan, M. O. Li, *Nature* **2023**, *619*, 616; d) J.-L. Liang, X.-K. Jin, G.-F. Luo, S.-M. Zhang, Q.-X. Huang, Y.-T. Lin, X.-C. Deng, J.-W. Wang, W.-H. Chen, X.-Z. Zhang, *ACS Nano* **2023**, *17*, 17217.

[4] S. Liu, P. Dharanipragada, S. H. Lomeli, Y. Wang, X. Zhang, Z. Yang, R. J. Lim, C. Dumitras, P. O. Scumpia, S. M. Dubinett, G. Moriceau, D. B. Johnson, S. J. Moschos, R. S. Lo, *Nat. Med.* **2023**, *29*, 1123.

[5] E. Y. Lin, A. V. Nguyen, R. G. Russell, J. W. Pollard, *J. Exp. Med.* **2001**, *193*, 727.

[6] S. Zielen, J. Trischler, R. Schubert, *Expert Rev. Clin. Immunol.* **2015**, *11*, 409.

[7] a) Y. Xue, X. Yan, D. Li, S. Dong, Y. Ping, *Nat. Commun.* **2024**, *15*, 2270; b) C. W. Shields, M. A. Evans, L. L.-W. Wang, N. Baugh, S. Iyer, D. Wu, Z. Zhao, A. Pusuluri, A. Ukidve, D. C. Pan, S. Mitragotri, *Sci. Adv.* **2020**, *6*, aaz6579.

[8] a) H. Cai, Y. Zhang, J. Wang, J. Gu, *Front. Immunol.* **2021**, 12; b) G. Hartley, D. Regan, A. Guth, S. Dow, *Cancer Immunol. Immunother.* **2017**, *66*, 523.

[9] a) L. Đorđević, F. Arcudi, M. Prato, *Nat. Protoc.* **2019**, *14*, 2931; b) L. Đorđević, F. Arcudi, M. Cacioppo, M. Prato, *Nat. Nanotechnol.* **2022**, *17*, 112.

[10] S. Li, W. Su, H. Wu, T. Yuan, C. Yuan, J. Liu, G. Deng, X. Gao, Z. Chen, Y. Bao, F. Yuan, S. Zhou, H. Tan, Y. Li, X. Li, L. Fan, J. Zhu, A. T. Chen, F. Liu, Y. Zhou, M. Li, X. Zhai, J. Zhou, *Nat. Biomed. Eng.* **2020**, *4*, 704.

[11] a) P. M. Kharkar, K. L. Kiick, A. M. Kloxin, *Chem. Soc. Rev.* **2013**, *42*, 7335; b) W. Sang, Z. Zhang, Y. Dai, X. Chen, *Chem. Soc. Rev.* **2019**, *48*, 3771.

[12] a) F. Wang, H. Su, D. Xu, W. Dai, W. Zhang, Z. Wang, C. F. Anderson, M. Zheng, R. Oh, F. Wan, H. Cui, *Nat. Biomed. Eng.* **2020**, *4*, 1090; b) Y. Chao, L. Xu, C. Liang, L. Feng, J. Xu, Z. Dong, L. Tian, X. Yi, K. Yang, Z. Liu, *Nat. Biomed. Eng.* **2018**, *2*, 611.

[13] a) L. Guo, X. Niu, X. Chen, F. Lu, J. Gao, Q. Chang, *Biomaterials* **2022**, *282*, 121406; b) S. Jalili-Firoozinezhad, S. Rajabi-Zeleti, P. Mohammadi, E. Gaudiello, S. Bonakdar, M. Solati-Hashjin, A. Marsano, N. Aghdami, A. Scherberich, H. Baharvand, I. Martin, *Adv. Healthcare Mater.* **2015**, *4*, 2281; c) K. Huang, J. Hou, Z. Gu, J. Wu, *ACS Biomater. Sci. Eng.* **2019**, *5*, 5384.

[14] a) Y. Liu, Z. Deng, J. Zhang, Y. Wu, N. Wu, L. Geng, Y. Yue, Q. Zhang, J. Wang, *Biomacromolecules* **2023**, *24*, 4831; b) Y. Yu, K. Dai, Z. Gao, W. Tang, T. Shen, Y. Yuan, J. Wang, C. Liu, *Sci. Adv.* **2021**, *7*, abd8217.

[15] a) B. Ma, X. Fu, P. Zhu, Z. Lu, J. Niu, F. Lu, *Crit. Rev. Food Sci. Nutr.* **2023**, *64*, 8672; b) P. Rupa, L. Schnarr, Y. Mine, *J. Funct. Foods* **2015**, *18*, 28.

[16] a) X. Ji, H. Lv, X. Sun, C. Ding, *Chem ChemComm* **2019**, *55*, 15101; b) Q. Luo, X. Huang, Y. Luo, H. Yuan, T. Ren, X. Li, D. Xu, X. Guo, Y. Wu, *Chem. Eng. J.* **2021**, *407*, 127050; c) X. Guo, D. Xu, H. Yuan, Q. Luo, S. Tang, L. Liu, Y. Wu, *J. Mater. Chem. A* **2019**, *7*, 27081.

[17] Y. Wang, T. Lv, K. Yin, N. Feng, X. Sun, J. Zhou, H. Li, *Small* **2023**, *19*, 2207048.

[18] X. Bao, Y. Yuan, J. Chen, B. Zhang, D. Li, D. Zhou, P. Jing, G. Xu, Y. Wang, K. Holá, D. Shen, C. Wu, L. Song, C. Liu, R. Zbořil, S. Qu, *Light-Sci. Appl.* **2018**, *7*, 91.

[19] H. H. Gustafson, D. Holt-Casper, D. W. Grainger, H. Ghandehari, *Nano Today* **2015**, *10*, 487.

[20] J. Wu, J. H. Lei, M. Li, A. Zhang, Y. Li, X. Liang, S. C. de Souza, Z. Yuan, C. Wang, G. Chen, T. M. Liu, C. X. Deng, Z. Tang, S. Qu, *Adv. Sci.* **2024**, *11*, 2404702.

[21] a) Y. Song, J. Jin, J. Li, R. He, M. Zhang, Y. Chang, K. Chen, Y. Wang, B. Sun, G. Xing, *J. Nanosci. Nanotechnol.* **2014**, *14*, 4022; b) J. Meng, X. Li, C. Wang, H. Guo, J. Liu, H. Xu, *ACS Appl. Mater. Interfaces* **2015**, *7*, 3180.

[22] a) J. Huang, L. Zhang, D. Wan, L. Zhou, S. Zheng, S. Lin, Y. Qiao, *Signal Transduct. Target Ther.* **2021**, *6*, 153; b) J. Winkler, A. Abisoye-Ogunniyan, K. J. Metcalf, Z. Werb, *Nat. Commun.* **2020**, *11*, 5120.

[23] Y. Gong, E. Hart, A. Shchurin, J. Hoover-Plow, *J. Clin. Invest.* **2008**, *118*, 3012.

[24] Y. Jiang, Q. Han, H. Zhao, J. Zhang, *J. Exp. Clin. Cancer Res.* **2021**, *40*, 13.

[25] B. Wu, J.-d. Liu, E. Bian, W. Hu, C. Huang, X. Meng, L. Zhang, X. Lv, J. Li, *Int. J. Biol. Sci.* **2020**, *16*, 671.

[26] D. B. Johnson, M. V. Estrada, R. Salgado, V. Sanchez, D. B. Doxie, S. R. Opalenik, A. E. Vilgelm, E. Feld, A. S. Johnson, A. R. Greenplate, M. E. Sanders, C. M. Lovly, D. T. Frederick, M. C. Kelley, A. Richmond, J. M. Irish, Y. Shyr, R. J. Sullivan, I. Puzanov, J. A. Sosman, J. M. Balko, *Nat. Commun.* **2016**, *7*, 10582.

[27] a) M. V. Dhodapkar, K. M. Dhodapkar, A. K. Palucka, *Cell Death Differ.* **2008**, *15*, 39; b) L. Chiossone, P.-Y. Dumas, M. Vienne, E. Vivier, *Nat. Rev. Immunol.* **2018**, *18*, 671.

[28] Z. Chen, L. Liu, R. Liang, Z. Luo, H. He, Z. Wu, H. Tian, M. Zheng, Y. Ma, L. Cai, *ACS Nano* **2018**, *12*, 8633.

[29] D. A. Mahvi, R. Liu, M. W. Grinstaff, Y. L. Colson, C. P. Raut, *CA Cancer J. Clin.* **2018**, *68*, 488.

[30] Q. Qian, J. Song, C. Chen, Q. Pu, X. Liu, H. Wang, *Biomater. Sci.* **2023**, *11*, 2678.

[31] K. Prasad, R. Zhou, R. Zhou, D. Schuessler, K. K. Ostrikov, K. Bazaka, *Acta Biomater.* **2019**, *86*, 41.